J. Cell Sci. **14**, 523–549 (1974)
Printed in Great Britain

ARRANGEMENT OF SUBUNITS IN FLAGELLAR MICROTUBULES

LINDA A. AMOS AND A. KLUG
MRC Laboratory of Molecular Biology, Hills Road, Cambridge CB2 2QH, U.K.

SUMMARY

Electron micrographs of outer doublet tubules from flagella have been analysed by methods which make use of the computed diffraction patterns of electron-microscope images. Analysis of singlet A-tubules in the tips of flagella has led to a determination of the helical surface lattice of the A-subfibre, confirming that there are 13 longitudinal protofilaments in the tubule wall and that dimers in neighbouring protofilaments form a staggered arrangement, equivalent to the lattice with an axial periodicity of 8·0 nm predicted in earlier work. A low-resolution 3-dimensional image of the A-tubule has been reconstructed, which supports the evidence for an 8·0-nm-long heterodimer oriented along the protofilaments. The heterodimer is identified as a pair of 4·0-nm morphological units, which appear to be globular at this resolution.

Filtered images have been obtained from doublet tubules which show that the B-subfibre is also made up of 8·0-nm dimers, but it differs from the A-tubule in that dimers in adjacent filaments are not in a staggered arrangement but are lined up obliquely at a shallow angle. Using the additional information about the hands of the lattices in the 2 subfibres which is presented in the accompanying paper, a model for the whole doublet has been proposed.

INTRODUCTION

The arrangement of the subunits within the outer and central tubules of flagella has been investigated previously by Grimstone & Klug (1966), who analysed electron micrographs of negatively-stained material from *Trichonympha* and other flagellates using the technique of optical diffraction. They concluded that the subunits comprising the walls of the tubules lie on a helical surface lattice with a period of 4·0 nm along its axis. Additional longitudinal periodicities of 8·0, 16·0 and 48·0 nm which are apparent in the optical diffraction patterns were thought to arise from perturbations in the arrangement of identical subunits and/or by the attachment of other components. A simple displacement in the relative positions of alternate subunits was suggested which would give rise to the observed 8·0-nm periodicity.

Tubulins

Since that time, much additional information about the components of cilia and flagella has emerged (for a review see Warner, 1972). In particular, the globular subunits which form the walls of both singlet and doublet tubules are now believed to be molecules of a class of proteins known as tubulins (Mohri, 1968; Stephens, 1970) which are also found in microtubules from other sources (see, for example, Renaud, Rowe & Gibbons, 1968; Weisenberg, Borisy & Taylor, 1968; Shelanski & Taylor, 1968; Stephens, 1970). Cytoplasmic microtubules readily dissociate into dimers of

about 110000 mol. wt. and under more drastic conditions monomers are formed with a molecular weight of approximately 55000. Flagellar tubules dissociate less readily, but under appropriate conditions, their tubulins can be prepared as monomers or dimers. It has been shown that in cytoplasmic tubules and in both A- and B-subfibres of flagellar doublet tubules the tubulin monomers consist of 2 different species in approximately equal amounts (Bryan & Wilson, 1971; Feit, Slusarek & Shelanski, 1971; Olmsted, Whitman, Carlson & Rosenbaum, 1971; Witman, 1970). Because of this Bryan & Wilson have postulated that the dimer of cytoplasmic tubules is a heterodimer of 2 different tubulins. It seems likely that flagellar tubules also consist of heterodimers, since this would give a natural explanation of the strong 8·0-nm period observed in intact tubules from all sources (Pease, 1963; André & Thiéry, 1963; Grimstone & Klug, 1966; Burton, 1970; Thomas, 1970). Witman, Carlson & Rosenbaum (1972) have found evidence that the 2 main species of tubulin in flagellar tubules may be further separated into at least five subspecies, but this result has not yet been confirmed by other workers.

The number of longitudinal protofilaments and their arrangement in the doublet tubules has been determined in several species from sectioned material (for example: Ledbetter & Porter, 1964; Phillips, 1966; Ringo, 1967; Warner & Satir, 1973). In most cases it appears that the A-subfibre is a complete tubule consisting of 13 protofilaments, while the B-subfibre is an incomplete C-shaped tubule which has only 10 protofilaments of its own and seems to share the 3 filaments of the A-tubule lying in the midwall of the doublet. The 3 shared filaments form what is known as the partition. These numbers have been confirmed by observations on unfixed, negatively-stained material: Erickson (1970)* and Warner & Satir (1973) have independently counted the numbers of protofilaments in favourable micrographs of collapsed and fraying flagellar and ciliary outer fibres.

Other components

Recent structural studies of embedded and sectioned specimens have clarified the relationship between the tubules and the other structural components of cilia and flagella. 'Radial links' or 'spokes' extending from the A-subfibre of each outer doublet into the centre of the axoneme have been found to occur either in pairs about 32·0 nm apart (Warner, 1970; Hopkins, 1970) or in triplets about 24·0 nm apart (Chasey, 1972*b*) along the tubule, with a distance of approximately 96 nm between the centres of the successive groups. Gibbons (1965) demonstrated that the A-subfibres of outer doublets were held together in a cylindrical array by some other component, and Stephens (1970, 1971) and Linck (1973) proposed that there is a component (nexin) bridging A-tubules at intervals of 96·0 nm. The spacing of these 2 components, the radial links and the nexin bridges, appears to determine the longitudinal repeat of the whole flagellum. Optical diffraction patterns of intact axonemes show a 96·0-nm system of layer lines† (R. W. Linck, unpublished work), and we have also found

* Paper presented to the 1970 Birmingham meeting of the Society for Experimental Biology.

† Layer line spacings referred to in this work, such as 8·0, 16·0 and 96·0 nm, are all based on assigning the value 4·0 nm to the longitudinal spacings of the basic tubulin lattice, which may not be exact for all species.

traces of a 96·0-nm periodicity in computed diffraction patterns of individual tubules.

The values reported for the longitudinal spacing of the 2 rows of 'arms' (dynein) on the A-tubule are rather variable, ranging from 12·0 to 24·0 nm (Grimstone & Klug, 1966; Hopkins, 1970; Warner, 1970; Chasey, 1972*b*). However, the clearest pictures (Chasey, 1972*b*; R. W. Linck, unpublished work) show what seem to be single rows of arms with a 24·0-nm spacing. Chasey has suggested that the apparently shorter spacings arise because the 2 rows of arms are not in register. The strong 16·0-nm periodicity seen in the diffraction patterns of flagellar tubules is probably due to extra components required to build doublet tubules, possibly accompanied by a perturbation in the packing of the tubules, since it has not been found in the diffraction patterns of the cortical singlets which surround the '9+2' arrangement in lung fluke sperm (H. P. Erickson, personal communication). Furthermore, it is found to be particularly strong near the partitions of doublets (Grimstone & Klug, 1966, fig. 12).

The 4·0- and 8·0-nm periodicities

The optical diffraction patterns from a wide variety of preparations seen in the electron microscope show very similar features. The most constant are the 2 strong pairs of peaks on the 4·0-nm layer line (see Figs. 2–4). As observed by Grimstone & Klug, central singlets and doublet A- and B-subfibres of *Trichonympha* flagella masked off separately or together all give rise to peaks in the same positions on the 4-nm layer line. Similar sets of peaks have also been observed in optical diffraction patterns from *Tetrahymena* (Chasey, 1972*a*), from sea-urchin sperm tails (electron micrograph by J. T. Finch from a preparation kindly supplied by Dr Mazia) and from reconstituted microtubules from chick brain (Erickson, 1974). Finally, the 4·0-nm layer line peaks obtained from fixed intact axonemes are also similar, except that they are broken up into smaller spots because of interference between the contributions from different tubules (compare figs. 19 and 21 of Grimstone & Klug, 1966).

The intensity distribution on the 8·0-nm layer line is much more variable, both in intensity and in the positions of the peaks. There may be several reasons for this. First, the variation may be due to different degrees of preservation; the 8·0-nm periodicity is often almost absent in disintegrating tubules, although in well preserved specimens it may be stronger than the 4·0-nm layer line (Grimstone & Klug, 1966). Secondly, there may be contributions from the second and third order harmonics of components attached at periods of 16·0 or 24·0 nm, which vary from specimen to specimen; and third, there appears to be a real difference between the surface lattices of A- and B-subfibres, as described below.

The organization of tubulin has been studied by Cohen and her colleagues by X-ray diffraction of oriented gels of A-subfibres from thermally fractionated sperm tail outer fibres (Cohen, Harrison & Stephens, 1971). The X-ray pictures show 4 orders of the 4·0-nm repeat and some traces of a weak 8·0-nm layer line. However, instead of showing 2 clear peaks on each side of the 4·0-nm layer line, as almost all optical diffraction patterns do, the X-ray pattern has an off-meridional streak centred roughly midway between the 2 expected positions. Cohen *et al.* conclude from this

that the surface lattice in their preparation may be different from that seen in the electron microscope and suggest that the difference is due to a rearrangement produced by the stains used in electron microscopy. This explanation seems unlikely, however, in view of the striking agreement on the 4·0-nm layer line between optical diffraction patterns of unfixed individual tubules and those of fixed intact axonemes (Grimstone & Klug, 1966). A more likely explanation is that the streak on the 4·0-nm layer line of the X-ray patterns corresponds to a smearing together of the two 4·0-nm layer line peaks due to disorientation. Such an effect is not unlikely for a wet gel preparation, in which the fibres are only roughly oriented parallel to each other. Furthermore, the weakness of the 8·0-nm layer line provides good evidence that the tubules in the X-ray preparation are less well preserved than the best ones seen in the electron microscope: the advantage of the electron microscope is that selected individual fibres or small well-aligned bundles can be studied.

Three-dimensional reconstruction by computer

The other development, besides the new chemical information, which allows an extension of the original analysis is the introduction of computer methods of image analysis and 3-dimensional image reconstruction from electron-microscope images (DeRosier & Klug, 1968). For the analysis the image is converted to an array of numbers by means of a microdensitometer, and its diffraction pattern, or Fourier transform, is calculated in the computer. Since the computed Fourier transform of an image provides the phases as well as the amplitudes of each peak in the diffraction pattern, computer analysis is of great assistance in indexing the layer lines. Once the pattern has been indexed, the periodic data may be extracted and recombined to produce a 3-dimensional density map of the subject. In the case of flagellar tubules, only the singlets have helical symmetry, so only they and not the doublets can be reconstructed in 3 dimensions from a single image (see DeRosier & Klug, 1968). For this purpose we have used micrographs of flagellar tips (Grimstone & Klug, 1966, figs. 9–11, and Fig. 1 of the present paper), where the outer fibres lose their B-subfibres and become singlet A-tubules. In the case of the doublet tubules, it has been possible to reconstruct filtered 2-dimensional images (Klug & DeRosier, 1966), from which the substructures of the A- and B-subfibres may be compared.

INDEXING OF THE DIFFRACTION PATTERNS OF SINGLET A-TUBULES

The theory relevant to the indexing of helical diffraction patterns is contained in papers by Cochran, Crick & Vand (1952) and Klug, Crick & Wyckoff (1958), while applications of the theory to subjects imaged in electron micrographs are discussed, for example, by Klug & Berger (1964), Moody (1967) and DeRosier & Moore (1970). It will be mentioned only in outline here.

A helical surface lattice is determined by the intersection of any 2 families of parallel helices. These need not be physically continuous helices of matter, but simply lines passing through equivalent points in each unit cell. In the case of microtubules the obvious choice for one family of helices is that defined by the longitudinal proto-

filaments. If there are n_l such helices and there is also a prominent oblique family of number n_p with a particular pitch, this will imply another family of helices with a similar pitch but opposite hand and of number $n_q = n_l - n_p$. It is convenient to describe the surface lattice by the notation (n_l, n_p, n_q). In the special case that the longitudinal helices are straight lines exactly parallel to the axis, as they are here, then the 2 oblique families have exactly the same pitch and give rise to peaks on the same layer line. Grimstone and Klug were able to define the general form of the helical surface lattice from the 2 sets of diffraction peaks on the 4·0-nm layer line without knowing the exact values of n_l, n_p and n_q, although n_l was thought to be about 12. However, for a 3-dimensional image reconstruction we need to know these parameters exactly.

In fact, each n-fold helical family gives rise to 2 main diffraction peaks equidistant from the meridian of the layer line, one being derived from the near side of the helix, the other from the far side. Since the position of each peak is related to the Bessel function $\mathcal{J}_n(2\pi Rr)$, where r is the helix radius, the value of n associated with each pair of peaks can be calculated approximately from the distance in reciprocal space (R) of the peaks from the meridian. Furthermore, the relative phase of the 2 peaks shows whether n is odd or even, since, if the phase origin is on the axis of the particle, the two spots should be exactly in phase for an even value of n, or exactly out of phase in the case of an odd value of n (see Finch & Klug, 1971).

The number of protofilaments

Fig. 2 shows a typical diffraction pattern (computed in this case) from a singlet A-tubule, with the computed phases marked alongside the main peaks under consideration. If we assume that the main density of the tubules lies between radii of 8·0 and 12·0 nm, the positions of the pair of peaks on the equator are such that n_l lies between 11 and 14. The computed phases at these points, which differ by about 180°, reduce this choice to an odd number, that is 11 or 13. In fact it is possible to deduce directly from the micrographs that the number of longitudinal filaments is odd. This is because most of the images show a left-right asymmetry about the tubule axis, with stronger longitudinal striations on one side (see Fig. 1). In negative stain bright striations are produced by the superposition of 2 filaments, so the fact that some images (e.g. particle A of Fig. 1) show 6 striations means that the number of protofilaments is almost certainly thirteen. This agrees with the results obtained by others (see Warner & Satir, 1973, for example).

The 4·0-nm layer line

The positions of the 2 pairs of strong peaks on the 4·0-nm layer line limit their possible Bessel orders to the ranges 2–4 and 6–12 respectively. The computed phases (Fig. 2) indicate an odd order, which must be 3, for the near meridional peak and an even order (6, 8, 10 or 12) for the outer peak. The only combination of values which defines a periodic reciprocal lattice consistent with the choice of 13 for n_l is $\bar{n}_p = \bar{3}$ and $n_q = 10$, as shown in Fig. 5A. (The sense of the helices, and hence the absolute

signs of the Bessel orders, have been determined from a series of views of tubules tilted in the electron microscope, as described in the following paper (Linck & Amos, 1974).)

The 8·0-nm layer line

Subdivision of the reciprocal lattice to give an 8·0-nm periodicity leads to values of $\bar{n}_p = \bar{8}$, $n_q = 5$ on the 8·0-nm layer line. Inspection of the computed 8·0-nm layer line shows a single long peak in a position consistent with values of n between 4 and 8. The phases differ by between 90 and 140°, suggesting that the peak consists of a mixture of functions. The effect of having 2 orders, differing numerically by only 1 or 3, on the same layer line has been discussed in detail for the case of bacterial flagella (Finch & Klug, 1972). It means that in the helical surface lattice there are an odd and an even family of helices, not only with the same pitch but also of similar azimuthal spacing. Since the electron-microscope image may be regarded as a superposition pattern of the near and far sides of the tubule, in certain orientations the n_p helices on one side will be approximately superimposed on the n_q helices of the same pitch on the other side, producing a set of strong oblique striations in the image. On the other hand, because one family has an odd and the other an even number of helices, the n_q helices of the first side and the n_p helices of the second side will be out of register and will not contribute significantly to the superposition pattern. The corresponding effect in the diffraction pattern is that the 2 functions on the layer line overlap to a certain extent. Since overlapping odd and even orders tend to reinforce on one side of the meridian and to cancel on the other over a wide range of orientations, the intensities on the 2 sides of the layer line may be very different. This would explain the apparent 'one-sidedness' of the 8·0-nm layer line in many transforms of images which otherwise appear to be 2-sided (see, for example, figs. 17 and 19 of Grimstone & Klug, 1966; Chasey, 1972*a*, fig. 2). Likewise, the obliquely striated images obtained by Thomas (1970) and Burton (1970) can be explained as superposition patterns in which the two 8·0-nm helical families from opposite sides are in register. It is not necessary to propose that images which do not show oblique striations are of a different structure, the so-called 'protofibrillar form' (Thomas, 1970), since they can be explained as superposition patterns of the 2 sides of the tubule for which no oblique helical families are quite in register.

The helical surface lattice

The diffraction pattern almost certainly corresponds to the indexing scheme shown in Fig. 5A. Fig. 6A shows the surface lattice derived from this, which agrees with the original lattice proposed by Grimstone & Klug (their fig. 1*b*), having the same staggered arrangement of pairs of 4·0-nm subunits in adjacent protofilaments. The main helices of the surface lattice are labelled with their values of n. Apart from the 13 longitudinal filaments, the main helices are a 3-start family with an azimuthal separation between members of 4·0 nm (sometimes called the minor pitch) and an angle of about 18° at a radius of 12·0 nm, together with a 5-start and an 8-start family each of 8·0-nm minor pitch. The heterodimers are represented by the dumb-bells which are made up of 2 almost equal 4·0-nm units (which Grimstone and Klug took to be 2

equal units in slightly different positions). The reason for believing that the 110000 mol. wt. dimers are oriented along the axis, rather than along the 4·0-nm period helices, is that when the tubules begin to disintegrate they fray readily into axial protofilaments, indicating that the lateral bonds are weaker than the longitudinal ones.

Possible incorporation of longer periodicities

It is possible to form larger unit cells in the surface lattice (and correspondingly smaller reciprocal cells) by attaching extra components to the tubule in a regular manner. The present 8·0-nm lattice could in fact be a sub-cell of a larger superlattice of period 96·0 nm, the axoneme repeat. In this case the $n-l$ plot would be subdivided as shown in Fig. 5A. A system of layer lines of 96·0-nm periodicity can be detected in the computed transforms; however, the phases of corresponding peaks on left and right hand sides are not correlated as expected for a true helical structure. The possible exception is the near meridional peak of the $1/5{\cdot}3$ nm^{-1} layer line (the 3rd order of a 16·0 nm period), where the phases would support the assignment of $n = 1$ (see Fig. 2). The possibility that the 16·0-nm period really is part of the helical surface lattice of the tubulin is still under investigation.

OPTICAL FILTERING OF SINGLET A-TUBULES

The overlap of the contributions from 2 different helical families on the 8·0-nm layer line and of the equatorial peaks diffracted by the longitudinal protofilaments on the near and far sides of the tubule means that straightforward 2-dimensional filtering to separate the images of the two sides, either optically (Klug & DeRosier, 1966) or by computer (Amos & Klug, 1972), is not strictly valid. However, because the overlap on the 8·0-nm layer line is not total, partial separation of the images of the near and far sides of the tubule may be achieved. Also, in cases where the protofilaments on the 2 sides of the tubule are exactly superimposed, the contribution to the equator from a single side can be obtained simply by reducing the transmission by one half.

Some trial optical filtering of suitable images produced results such as those shown in Figs. 3 and 4. The 2 filtered images show 8-nm dimers but are so different that, without the 3-dimensional analysis described below, one could have little confidence in either result. These reservations apply equally to the work of Chasey (1972*a*), who moreover interpreted his diffraction patterns in terms of a model based on 12 protofilaments, which does not agree with our analysis.

THREE-DIMENSIONAL IMAGE RECONSTRUCTION OF THE A-TUBULE

A 3-dimensional image of the singlet A-tubules shown in Fig. 1 has been reconstructed using data from the 4·0- and 8·0-nm layer lines and the equator. The procedure followed was basically that described by DeRosier & Moore (1970) for particles with helical symmetry. No attempt has been made to include the intermediate layer lines, which probably arise from the attachment of extra components to the basic tubule, since it is unlikely that all these components are arranged with helical symmetry.

Processing of layer line data

The data were selected from the transform of each electron-microscope image and their phases corrected for errors in orientation as described by DeRosier & Moore (1970). Only the equator and the 4·0-nm layer line could be used in the refinement of the position of the phase origin (i.e. fixing the position of the helical axis in the image) and for estimating the angle of tilt of the particles out of the projection plane. It was not possible to identify pure 5-fold and 8-fold harmonics on the 8·0-nm layer line; however, the odd and even components could be separated by taking vector sums and differences of the 2 sides of the layer line.* This separation was performed after the refinement of the phase origin. An example of the process is shown in Fig. 7. This procedure was carried out assuming that the lack of phase correlation on the left and right sides of the layer line arises from the overlap of only 2 functions. It is possible, however, that there are contributions from other orders, such as the second harmonics of a non-helical 16·0-nm period. It has also been suggested (Witman *et al.* 1972) that the tubulin dimers in different protofilaments differ slightly. In either case, the effect of attributing the data entirely to 5-fold and 8-fold cylindrical harmonics would be to produce in the reconstruction an average protofilament, which is the best that can be done using a single view of a particular tubule.

On the equator there are overlapping Bessel contributions of order ± 13 (see Fig. 5A), which must also be separated before being incorporated into a 3-dimensional reconstruction.† In theory, data from at least 2 different images of known relative orientation are needed for this, since only 2 orders of different parity can be sorted out from a single transform plane. In practice, the process of separating the 2 terms using data from different transforms is subject to large error, for the results are strongly dependent upon having the data from different images on exactly the same scale. Because of this difficulty the separation was finally made by assuming that the most strongly longitudinally striated image seen corresponded to a section through the 3-dimensional Fourier transform where the two 13-fold cylindrical harmonics reinforced exactly.

Comparison and averaging of different sets of data

Three of the best images were selected on the basis of the phase correlation between opposite sides of their 4·0-nm layer lines and the strength of their 8·0-nm layer lines. The relative orientations of the images were determined by calculating the change in orientation which would theoretically produce the best agreement between phases on the 4·0-nm and 8·0-nm layer lines in different transforms. After correcting the phases to allow for these differences in orientation, the different sets of data were compared using methods which will be described in detail elsewhere (L. A. Amos, paper in preparation). A 'residual' calculated from the differences in the 2 sets of phases provides some indication of the degree to which different sets of data are equivalent. (For completely random data one might expect a mean phase difference of 90°.) Table 1 shows the phase residual (amplitude weighted) of the individual transforms when compared with the average of the three.

The residuals show that there is good agreement amongst the 3 data sets on the 4·0-nm layer

* The complex function, distance R from the meridian, on the 8·0-nm layer line has the form

$$F(R,\Phi) = G_5(R)\exp[i5(\Phi+\tfrac{1}{2}\pi)] + G_{\bar{5}}(R)\exp[-i8(\Phi+\tfrac{1}{2}\pi)].$$

For points to the right of the meridian, we take $\Phi = \frac{1}{2}\pi$; and to the left, $\Phi = -\frac{1}{2}\pi$. Thus,

$$F(R,\tfrac{1}{2}\pi)+F(R,-\tfrac{1}{2}\pi) = 2G_{\bar{8}}(R),$$
$$F(R,\tfrac{1}{2}\pi)-F(R,-\tfrac{1}{2}\pi) = 2G_5(R)$$

† The combination of the 2 cylindrical harmonics of indices 13 and $\overline{13}$ on the equator has the form $2i\mathcal{J}_{13}(2\pi Rr)\sin(13\Phi)$. It therefore has a constant phase of 90° or 270°, and varies only in amplitude as the view angle Φ is changed. The observed differences in the phases from 90° and 270° respectively (Fig. 2) can be accounted for by the contribution from the equatorial $\mathcal{J}_0$ term.

line. The data on the 8·0-nm layer line are obviously inferior and this is probably due to the build-up of errors during the process of separating the J_5 and J_8 contributions. Even so, the results are compatible with those for other biological assemblies studied in this laboratory by ourselves and our colleagues.

Table 1. *Phase residuals obtained when different sets of data are compared with their average*

Particle	4·0-nm layer line	8·0-nm layer line	4·0-nm + 8·0-nm layer lines
A	4°	47°	35°
F	11°	33°	23°
H	11°	37°	27°

Test for polarity

In order to see whether the difference between the 2 halves of a dimer was significant, or whether the structure should be regarded as non-polar, a search was made in the computer for the best approximation to a 2-fold axis, normal to the axis of the tubule. In a true 2-fold orientation, the layer line data in the transform should all be real; therefore the differences in the phases from either 0° or 180° give an indication of how far the structure is from being exactly 2-fold. A '2-fold phase residual' was calculated for each set of data from individual tubules used in the reconstruction and from their average. Whereas the residual was about 40° for individual images, it was about 54° for the average, showing that averaging out random noise had slightly increased the apparent amount of polarity. This may be compared with the case of haemocyanin (Mellema & Klug, 1972) which is believed to possess a true dyad. When the above process was applied to haemocyanin data, averaging of data from different particles significantly reduced the apparent polarity. We conclude that the polarity of the microtubule, although relatively small at this low resolution, is not an artifact.

RESULTS OF THE THREE-DIMENSIONAL IMAGE RECONSTRUCTION

Fig. 13 shows a model of the 3-dimensional reconstruction synthesized from the averaged data, while Figs. 8 and 9 show the density distribution in more detail, in the form of sections through the reconstructed tubule. We have actually reconstructed the distribution of the electron-dense stain around the microtubules and interpret holes in the stain as protein. At such low resolution, the boundaries between stain and protein are not very sharply defined; therefore the contour level which defines the boundary of the model has been chosen so that the volume within a 4·0-nm morphological unit is consistent with a molecular weight of about 55000 and an assumed density of 1300 mol. wt. nm^{-3} (see Mikhailov & Vainshtein, 1971). A small column of density appearing on the axis of the tube was judged to be an artifact, since errors such as those arising from the lack of cylindrical symmetry of the negative stain would build up here. It has been omitted from the model.

As one would expect from the original micrographs, the strongest feature of the reconstructed model is the separation of the tubule wall into longitudinal protofilaments. Alternate morphological units in each protofilament, which we designate α-subunits (although they may not in fact correspond to the chemical monomers (see below)), project outwards more than the others (Figs. 8, 9); while on the inside there

are sharp projections from the second type of subunit (labelled β). The difference in the radial position of the 2 types of subunit results in the zig-zag appearance of Fig. 9, which shows a central section through part of a protofilament. It is possible that the outward projections of the α-subunits are really as sharp as the inward projections of the β-subunits, but that these details are obscured in the image by the relatively greater thickness of negative stain on the outside.

Lateral connexions between different subunits appear to be much less substantial than the longitudinal ones. The strong dimer bond is thus most likely to be in the longitudinal direction, as suggested by the manner in which the tubules fray. Alternate longitudinal connexions between the 4-nm morphological units have a slightly higher density, so we identify the dimer as being a pair of α and β subunits, such as those shown shaded in Figs. 8, 9. In projection the pair of subunits would appear as a dumb-bell, as in the filtered image of Fig. 3.

ANALYSIS OF DOUBLET TUBULES

Diffraction patterns of doublet tubules

As described by Grimstone & Klug, the diffraction patterns from doublets are very similar to those from the singlet tubules, except that the layer lines tend to be broken up into a larger number of peaks (see Fig. 10B). The effect is particularly noticeable on the 8·0-nm layer line and was attributed to interference between the contributions from the 2 subfibres. We now know that the main reason for the complexity of the 8·0-nm layer line of doublets is that the A- and B-subfibres give rise to peaks in different positions, corresponding to 2 different surface lattices. This is shown by masking off the A- and B-subfibres separately. It is not easy to obtain good diffraction patterns optically, but portions of digitized images may be masked off very accurately to give reasonably good computed diffraction patterns. Figs. 10D and E show computed patterns from the A- and B-subfibres of the image in Fig. 10A. Each subfibre was masked so as to include half of the partition region. Although the peaks on the equators and the 4·0-nm layer lines, are very similar, the two 8·0-nm layer lines are quite different. The diffraction pattern from the A-subfibre is consistent with those from singlet A-tubules (see Figs. 2–4), forming the reciprocal lattice OPRS of Fig. 10B. The B-subfibre, on the other hand, produces peaks close to the meridian on the 8·0-nm layer line (e.g. the peak labelled M in Fig. 10E), which define the lattice OQSR. Thus, the reciprocal lattices of the A- and B-subfibres are quite different, although they pass through the same points on the 4·0-nm layer line and the equator.

The 2 reciprocal lattices are compared in Figs. 5A and B. Although the B-subfibre is not a complete tubule, it is convenient in the discussion below to refer to its lattice in terms of the helical families it would have had if it were a complete tubule of 13 protofilaments like the A-subfibre. This terminology is quite natural for the 4·0-nm lattice, which has the same angles and spacings in the 2 subfibres. However, when we come to 'index' the 8·0-nm layer line of the B-subfibre we must use half-integral values of n, as shown in Fig. 5B.

Filtered images of doublet tubules

As in the case of the singlet A-tubules, separation of the 2 sides of the image by optical filtering is successful only in favourable cases, such as that shown in Fig. 11. Figs. 11 C and E show filtered images obtained using the filtering masks illustrated in Figs. 11 B and D. Each image is believed to contain contributions mainly from one side of the doublet, either the front or the back. The identification of the different peaks on the 8·0-nm layer line was made by comparing the diffraction patterns of the individual subfibres with that of the doublet, as described for Fig. 10. The difference in the arrangement of dumb-bell-shaped dimers in the 2 subfibres is quite clear: in the A-subfibre there is the same staggered pattern as in the wall of the singlet A-tubules; in the B-subfibre, on the other hand, the dimers are not staggered, but line up along the direction of the 3-start helices of 4·0-nm minor pitch.

The examples shown in Figs. 10 and 11 are both taken from *Trichonympha*, but we have confirmed that the unexpected difference between the A- and B-subfibres occurs in other species. A particularly good example of the B lattice comes from a collapsed and opened out specimen from *Tetrahymena* flagella photographed by H. P. Erickson. This is shown in Fig. 12 A. Since in this case the image is simply one-sided there is no problem of separating different contributions, so the result is more reliable. (Unfortunately the 8·0-nm periodicity is preserved in opened out sheets only in rare instances. A sufficiently well-preserved opened out A-tubule has not yet been found.) Fig. 12 B shows the diffraction pattern obtained from the area outlined in Fig. 12 A, and 12 C is the noise-filtered image, which shows an arrangement of 8·0-nm units of the same kind as that found for the B-subfibre of *Trichonympha* (Fig. 11).

Model of a doublet tubule

Optical filtering does not of course determine the hand of a structure, nor even the relative hands of the A- and B-subfibres of the doublet. The hand can only be determined by tilting the specimen in the microscope and this has been done, as described in the following paper (Linck & Amos, 1974). The results of that study show that the 3-start helices of 4·0-nm minor pitch are left-handed in both subfibres. The situation shown in Fig. 12 A of the present paper provides some support for this result in the case of the B-subfibre. Since the B-subfibre has apparently fallen away from the A-subfibre and opened out after landing on the carbon film, one would expect the outer surface to be in contact with the carbon. This assumption leads to the assignment of a left-handed sense to the 3-start 4·0-nm helices (the printing convention used here is such that the specimens are seen from the side nearest to the grid).

This knowledge, together with the filtered images of Fig. 11, enables us to construct a scheme for the arrangement of dimers in the doublet tubules. Of the several possible relationships between the A and B lattices, the arrangement which agrees best with the filtered images is shown in Fig. 14, where the rows of B-subfibre dimers line up approximately with the nearest A-subfibre dimers at the 2 'seams' joining the subfibres. A less likely alternative is one in which the 8·0-nm lattices in the 2 subfibres are shifted relative to one another longitudinally by 4·0 nm. In either case, the 4·0-nm

lattice, being of the same hand in both subfibres, is approximately continuous across both seams. Fig. 6B represents the first model and shows the B-subfibre opened up and seen from the inside. The 'partition', or common wall, is represented by 3 A-tubule protofilaments, with their dimers in the staggered arrangement of Fig. 6A. The 10 protofilaments of the B-subfibre, on the other hand, have an unstaggered arrangement of dimers. There is no obvious structural reason for this difference between the 2 lattices, since it does not appear to allow them to intermesh any more easily.

DISCUSSION

At the limit of resolution of the present study, i.e. 4·0 nm, the A-tubule appears to be made up of tilted dumb-bell-shaped dimers, which are joined end-to-end to form longitudinal protofilaments. The arrangement of the 4·0-nm morphological units shown in the model (Fig. 13) is very similar to that which arises by perturbing a perfect lattice of 4·0-nm units in the way suggested by Grimstone & Klug (1966), although the main perturbation is radial rather than azimuthal as depicted in fig. 1*b* of that paper. A radial perturbation was also suggested at that time but could not be drawn easily.

Information about the 3-dimensional density distribution in the A-tubules has been obtained mainly from the singlet stretches at the tips of flagella. But since there is no apparent discontinuity in the A-tubule at the point where the B-subfibre ends (see Fig. 1), the structure is assumed to be the same in the rest of the A-subfibre. There is further evidence for this in that the diffraction patterns from both regions of the A-tubule are very similar.

We have tentatively labelled the 2 halves of the 8·0-nm dumb-bells α and β, but these may not really correspond to the 2 kinds of chemical monomer. Warner & Meza (1972) have noted a chain-like appearance of individual protofilaments in broken down flagellar tubules, and Erickson (1974, and personal communication) has demonstrated a longitudinal splitting of the 4·0-nm units, both in flagellar outer doublets and in purified sheets of tubulin from chick brain. This raises the possibility that the dimers are divided into two along their axes rather than into separate α and β morphological units as shown here. Unfortunately, the resolution so far obtained from averaging over relatively long lengths of intact tubules, as is done in 3-dimensional reconstruction, is insufficient to detect this feature. However, we have probably identified the dimer itself correctly: as discussed above, the dimer is almost certainly confined to a single protofilament and the known molecular weight is only consistent with a dimer which occupies the volume enclosed by at least two of the 4·0-nm subunits. It is not possible to decide from the reconstruction whether the dumb-bells represent a heterodimer or whether they are homodimers whose halves are packed in a perturbed manner. The tilting of the dumb-bells leads to a structure with a distinct polarity, which tends to support the chemical evidence for a heterodimer. But on the other hand, an alternation of 2 kinds of homodimer could be correlated with the 16·0-nm period which is found even in singlet A-tubules.

The 3-dimensional reconstructed image of the A-tubule provides a standard against which 2-dimensionally filtered images of doublet tubules may be compared. As

described above, filtering of the A-tubule to obtain a view of a single side is particularly difficult because of the overlap of different contributions to the 8·0-nm layer line, which will be different at different azimuths of view. Comparison of the filtered images with the 3-dimensional image shows which results are more reliable; thus the filtered image of Fig. 3 is more successful than that of Fig. 4. The B-subfibres can be more easily filtered, since the contributions to the 8·0-nm layer line are well separated here. In this case one may use the criterion that one would expect to find similar features (namely the dumb-bell-shaped units) in the images of both subfibres. On this basis, the filtered images of Fig. 11 appear to be reasonably reliable representations of the 2 sides of a doublet. The filtered image of a collapsed B-subfibre in Fig. 12C, which did not require the separation of the images of 2 overlapping surfaces, confirms the results from the intact tubules.

The striking feature of the doublet tubules is that, even though the lattices of the two subfibres are different at the 8·0-nm level of detail, at the 4·0-nm level they are effectively identical, even in their handedness. This means that, if we postulate that the dimers are heterodimers and are chemically similar in both subfibres, then lateral bonds between adjacent unlike subunits in the A-subfibre appear to be very similar to those between like subunits in the B-subfibre. It would suggest that all of the 4·0-nm morphological units are very similar, at least in their lateral bonding properties. This would favour the identification of the globular units with the chemical monomer and would require that the dimer be a polar arrangement of the 2 different kinds of monomer. The longitudinal splitting of the 4·0-nm units observed by Warner & Meza (1972) and Erickson (1974) may therefore simply be a cleft between 2 parts of the same molecule.

The difference in the 8·0-nm lattices of the 2 subfibres may be due to some subtle differences in the chemical properties of the tubulin dimers. However, although the properties of tubulins must determine the bonding pattern at a local level, it is unlikely that the overall shape of the doublet tubule can be explained in terms of tubulin chemistry. Other proteins must be involved in the higher level of organization required to attach the incomplete C-shaped B-subfibre to a specific region of the A-tubule and may even influence the packing arrangement of the 8·0-nm dimers. The partition appears to be built up from several proteins in addition to tubulins (R. W. Linck, paper in preparation), so quite possibly it is these minor protein components attached to the partition which dictate the relationship between the A- and B-subfibres. Clearly the partition needs to be studied in much greater detail, and particularly the 16·0-nm periodicity which emanates from it.

We thank Dr A. V. Grimstone for the use of the electron micrographs of *Trichonympha* flagellar tubules (Grimstone & Klug, 1966) and Dr H. P. Erickson for the micrograph of *Tetrahymena* tubules shown in Fig. 12A.

NOTE ADDED IN PROOF

Electron micrographs of sectioned axonemes published recently by Tilney *et al.* (*J. Cell Biol.* (1973) **59**, 267–275), who used an improved method of staining and fixation, confirm that the number of protofilaments in the A-subfibre is 13, but

suggest that the number in the B-subfibre may be 11 rather than 10. However, an extra protofilament in the B-subfibre would only affect the arrangements of subunits at the points where the B-subfibre is joined to the A-subfibre, which are not well defined in our present model.

REFERENCES

AMOS, L. A. & KLUG, A. (1972). Image filtering by computer. *Proc. 5th Europ. Congr. Electron Microsc.* (ed. V. E. Cosslett), pp. 580–581. London: Institute of Physics.

ANDRÉ, J. & THIÉRY, J. P. (1963). Mise en évidence d'une sous-structure fibrillaire dans les filaments axonématiques des flagelles. *J. Microscopie* **2**, 71–80.

BRYAN, J. & WILSON, L. (1971). Are cytoplasmic microtubules heteropolymers? *Proc. natn. Acad. Sci. U.S.A.* **68**, 1762–1766.

BURTON, P. R. (1970). Optical diffraction and translational reinforcement of microtubules having a prominent helical wall structure. *J. Cell Biol.* **44**, 693–699.

CASPAR, D. L. D. (1966). An analogue for negative staining. *J. molec. Biol.* **15**, 365–371.

CHASEY, D. (1972*a*). Subunit arrangement in ciliary microtubules from *Tetrahymena pyriformis*. *Expl Cell Res.* **74**, 140–146.

CHASEY, D. (1972*b*). Further observations on the ultrastructure of cilia from *Tetrahymena pyriformis*. *Expl Cell Res.* **74**, 471–479.

COCHRAN, W., CRICK, F. H. C. & VAND, V. (1952). The structure of synthetic polypeptides. I. The transform of atoms on a helix. *Acta crystallogr.* **5**, 581–586.

COHEN, C., HARRISON, S. C. & STEPHENS, R. E. (1971). X-ray diffraction from microtubules. *J. molec. Biol.* **59**, 375–380.

DEROSIER, D. J. & KLUG, A. (1968). Reconstruction of three-dimensional structures from electron micrographs. *Nature, Lond.* **217**, 130–134.

DEROSIER, D. J. & MOORE, P. B. (1970). Reconstruction of three-dimensional images from electron micrographs of structures with helical symmetry. *J. molec. Biol.* **52**, 355–369.

ERICKSON, H. P. (1974). Microtubule surface lattice and subunit structure and observations on reassembly. *J. Cell Biol.* **60**, 153–167.

FEIT, H., SLUSAREK, L. & SHELANSKI, M. L. (1971). Heterogeneity of tubulin subunits. *Proc. natn. Acad. Sci. U.S.A.* **68**, 2028–2031.

FINCH, J. T. & KLUG, A. (1966). Arrangement of protein subunits and the distribution of nucleic acid in turnip yellow mosaic virus. *J. molec. Biol.* **15**, 344–364.

FINCH, J. T. & KLUG, A. (1971). Three-dimensional reconstruction of the stacked-disk aggregate of tobacco mosaic virus from electron micrographs. *Phil. Trans. R. Soc. Lond. Ser. B* **261**, 211–219.

FINCH, J. T. & KLUG, A. (1972). The helical surface lattice of bacterial flagella. In *The Generation of Subcellular Structures*, First John Innes Symp., Norwich (ed. R. Markham & J. B. Bancroft), pp. 167–177. Amsterdam: North Holland Publishing.

GIBBONS, I. R. (1965). Chemical dissection of cilia. *Archs Biol., Liège* **76**, 317–352.

GRIMSTONE, A. V. & KLUG, A. (1966). Observations on the substructure of flagellar fibres. *J. Cell Sci.* **1**, 351–362.

GOSSLING, T. H. (1967). Two methods of presentation of electron density maps using a small-store computer. *Acta crystallogr.* **22**, 465–468.

HOPKINS, J. M. (1970). Subsidiary components of the flagella of *Chlamydomonas reinhardii*. *J. Cell Sci.* **7**, 823–839.

KLUG, A. & BERGER, J. E. (1964). An optical method for the analysis of periodicities in electron micrographs, with some observations on the mechanism of negative staining. *J. molec. Biol.* **10**, 565–569.

KLUG, A., CRICK, F. H. C. & WYCKOFF, H. W. (1958). Diffraction by helical structures. *Acta crystallogr.* **11**, 199–213.

KLUG, A. & DEROSIER, D. J. (1966). Optical filtering of electron micrographs: reconstruction of one-sided images. *Nature, Lond.* **212**, 29–32.

LEDBETTER, M. C. & PORTER, K. R. (1964). Morphology of microtubules of plant cells. *Science, N.Y.* **144**, 872–874.

LINCK, R. W. (1973). Chemical and structural differences between cilia and flagella from the lamellibranch mollusc, *Aequipecten irradians*. *J. Cell Sci.* **12**, 951–981.

LINCK, R. W. & AMOS, L. A. (1974). The hands of the helical lattices in flagellar doublet microtubules. *J. Cell Sci.* **14**, 551–559.

MELLEMA, J. E. & KLUG, A. (1972). Quaternary structure of gastropod haemocyanin. *Nature, Lond.* **239**, 146–150.

MIKHAILOV, A. M. & VAINSHTEIN, B. K. (1971). Electron microscope determination of the three-dimensional structure of the extended tail of the T6 bacteriophage. *Soviet Phys. Crystallogr.* **16**, 428–436.

MOHRI, H. (1968). Amino-acid composition of 'tubulin' constituting microtubules of sperm flagella. *Nature, Lond.* **217**, 1053–1054.

MOODY, M. F. (1967). Structure of the sheath of bacteriophage T4. I. Structure of the contracted sheath and polysheath. *J. molec. Biol.* **25**, 167–200.

OLMSTED, J. B., WHITMAN, G. B., CARLSON, K. & ROSENBAUM, J. L. (1971). Comparison of the microtubule proteins of neuroblastoma cells, brain, and *Chlamydomonas* flagella. *Proc. natn. Acad. Sci. U.S.A.* **68**, 2273–2277.

PEASE, D. C. (1963). The ultrastructure of flagellar fibrils. *J. Cell Biol.* **18**, 313–326.

PHILLIPS, D. M. (1966). Substructure of flagellar tubules. *J. Cell Biol.* **31**, 635–638.

RENAUD, F. L., ROWE, A. J. & GIBBONS, I. R. (1968). Some properties of the protein forming the outer fibres of cilia. *J. Cell Biol.* **36**, 79–90.

RINGO, D. L. (1967). The arrangement of subunits in flagellar fibres. *J. Ultrastruct. Res.* **17**, 266–277.

SHELANSKI, M. L. & TAYLOR, E. W. (1968). Properties of the protein subunit of central-pair and outer doublet microtubules of sea urchin flagella. *J. Cell Biol.* **38**, 304–315.

STEPHENS, R. E. (1970). Thermal fractionation of outer fibre doublet microtubules into A- and B-subfibre components: A- and B-tubulin. *J. molec. Biol.* **47**, 353–363.

STEPHENS, R. E. (1971). Microtubules. In *Biological Macromolecules*, vol. 5 (ed. S. Timasheff & G. D. Fasman), pp. 355–391. New York: Marcel Dekker.

THOMAS, M. B. (1970). Transitions between helical and protofibrillar configurations in doublet and single microtubules in spermatozoa of *Stylochus zebra*. *Biol. Bull. mar. biol. Lab., Woods Hole* **138**, 219–234.

WARNER, F. D. (1970). New observations on flagellar fine structure: the relationship between matrix structure and the microtubule component of the axoneme. *J. Cell Biol.* **47**, 159–182.

WARNER, F. D. (1972). Macromolecular organisation of eukaryotic cilia and flagella. In *Advances in Cell and Molecular Biology*, vol. 2 (ed. E. J. Du Praw), pp. 192–235. New York: Academic Press.

WARNER, F. D. & MEZA, I. (1972). Macromolecular and biochemical aspects of microtubule protofilaments. *J. Cell Biol.* **55**, 273*a*.

WARNER, F. D. & SATIR, P. (1973). The substructure of ciliary microtubules. *J. Cell Sci.* **12**, 313–326.

WEISENBERG, R. C., BORISY, G. G. & TAYLOR, E. W. (1968). The colchicine-binding protein of mammalian brain and its relation to microtubules. *Biochemistry, N.Y.* **7**, 4466–4478.

WITMAN, G. B. (1970). Fractionation and biochemical characterisation of the flagella of *Chlamydomonas reinhardii*. *J. Cell Biol.* **47**, 229*a*.

WITMAN, G. B., CARLSON, K. & ROSENBAUM, J. L. (1972). *Chlamydomonas* flagella. II. The distribution of tubulins 1 and 2 in the outer doublet microtubules. *J. Cell Biol.* **54**, 540–555.

(*Received* 16 *August* 1973)

Fig. 1. Electron micrograph showing tubules at the tip of a flagellum from *Trichonympha* (Grimstone & Klug, 1966). Arrows indicate points where the B-tubule of a doublet ends, while the A-tubule continues as a singlet. Lengths of A-tubule used in the 3-dimensional reconstruction are marked A, F and H. The computed Fourier transform of A is shown in Fig. 2. A is a strongly striated image, indicating that protofilaments on the near and far sides of the tubule are superimposed, while F has a smooth appearance because the protofilaments of near and far sides are out of register. H is intermediate between A and F. The tubule marked * is a particularly good illustration of the lack of mirror symmetry in the images, which shows that the number of protofilaments is odd. The maximum number of bright longitudinal striations that can be counted, e.g. in A, is 6. Since a single protofilament at the edge would hardly be seen (see Finch & Klug, 1966; Caspar, 1966), the number of protofilaments is deduced to be 13. × 100000.

Fig. 2. The computed diffraction pattern of a singlet A-tubule (stretch A of Fig. 1). A printout of the array of amplitudes in a 256 × 256 point transform, with contours drawn around the peaks; layer line spacings are in Ångstroms (0·1 nm). The phases (in degrees) of the important peaks are given above each peak. Only half of the diffraction pattern is shown, the origin being at the centre of the lower edge.

Fig. 3. An enlargement of the stretch of A-tubule marked 'A' in Fig. 1 (× 400000), together with its optical diffraction pattern and a filtered image. The filtered image was produced using the mask drawn on the diffraction pattern, with which it was hoped to include contributions from only one side of the tubule. In the lower part of the filtered image, the 8·0-nm periodicity is very weak and the 4·0-nm helices (marked $\bar{3}$) can easily be followed. In the rest of the image the 8-nm periodicity dominates, giving rise to dumb-bell-shaped units. This appearance is in agreement with the results of 3-dimensional reconstruction, which suggests that the second side of the image has been successfully filtered out. The 8·0-nm helices of dimers are marked by the number 5, the index for this family (see Fig. 5A).

Fig. 4. An electron micrograph of another example of a singlet A-tubule from a field similar to Fig. 1 (× 400000), together with its optical diffraction pattern and a filtered image obtained by masking the diffraction pattern as shown. In the filtered image, the appearance of the dimer is different from that in Fig. 3, being a pair of dots with one larger and brighter than the other, instead of resembling a dumb-bell. Because this does not agree in detail with the results of the 3-dimensional reconstruction it is possible that the image still includes a contribution from the 8·0-nm periodicity of the second side.

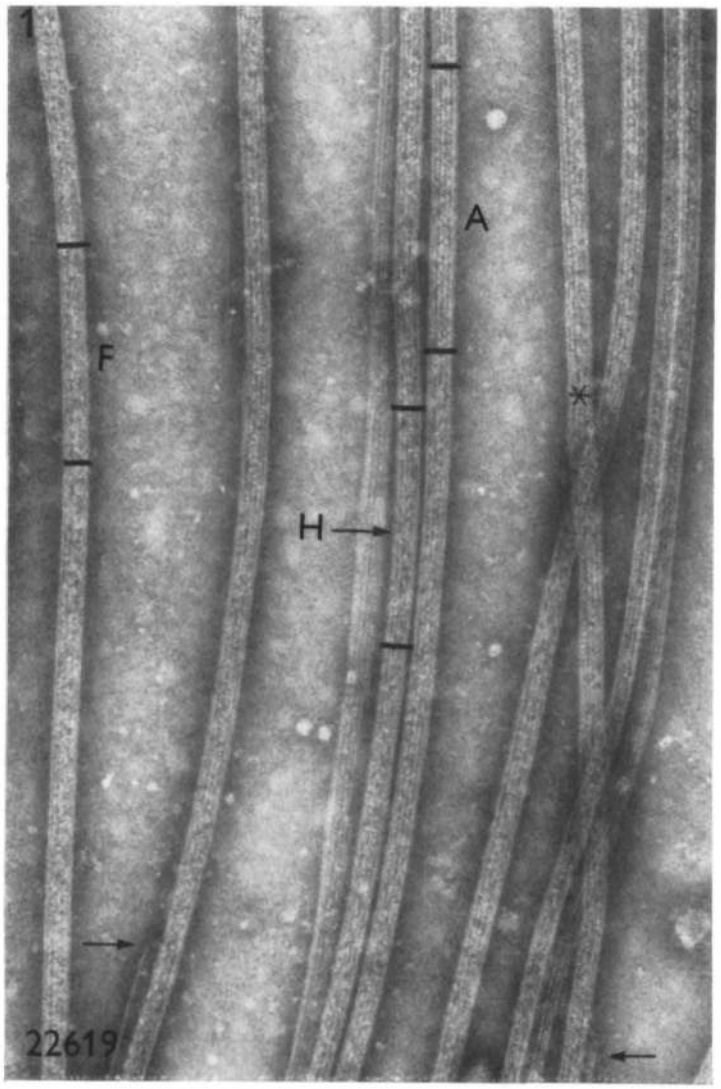
1
A
F
H
22619

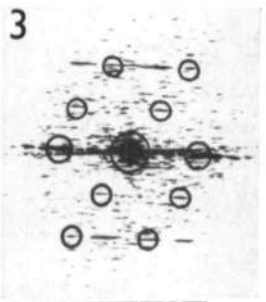
3

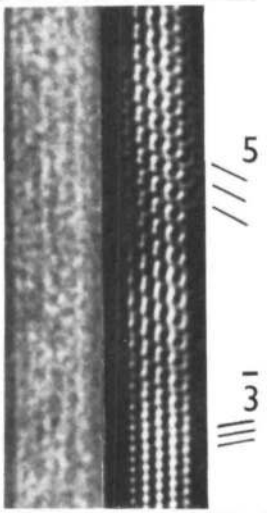
5
3

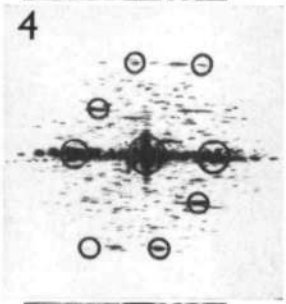
4

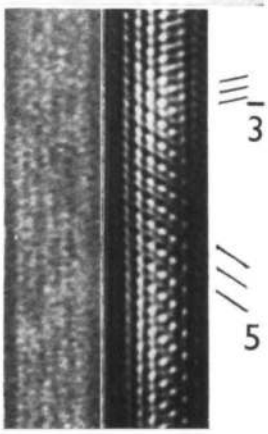
3
5

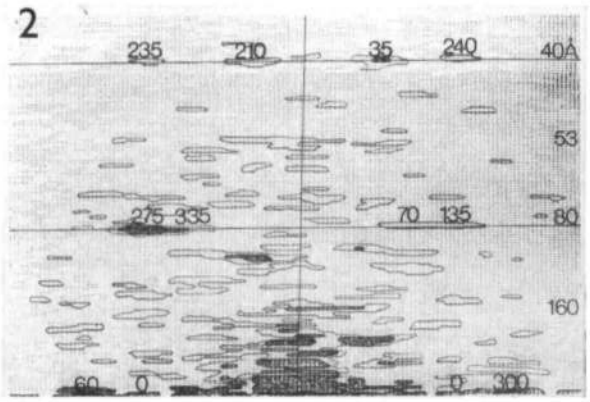
2
235
210
35
240
40Å
53
275
335
70
135
80
160
60
0
0
300

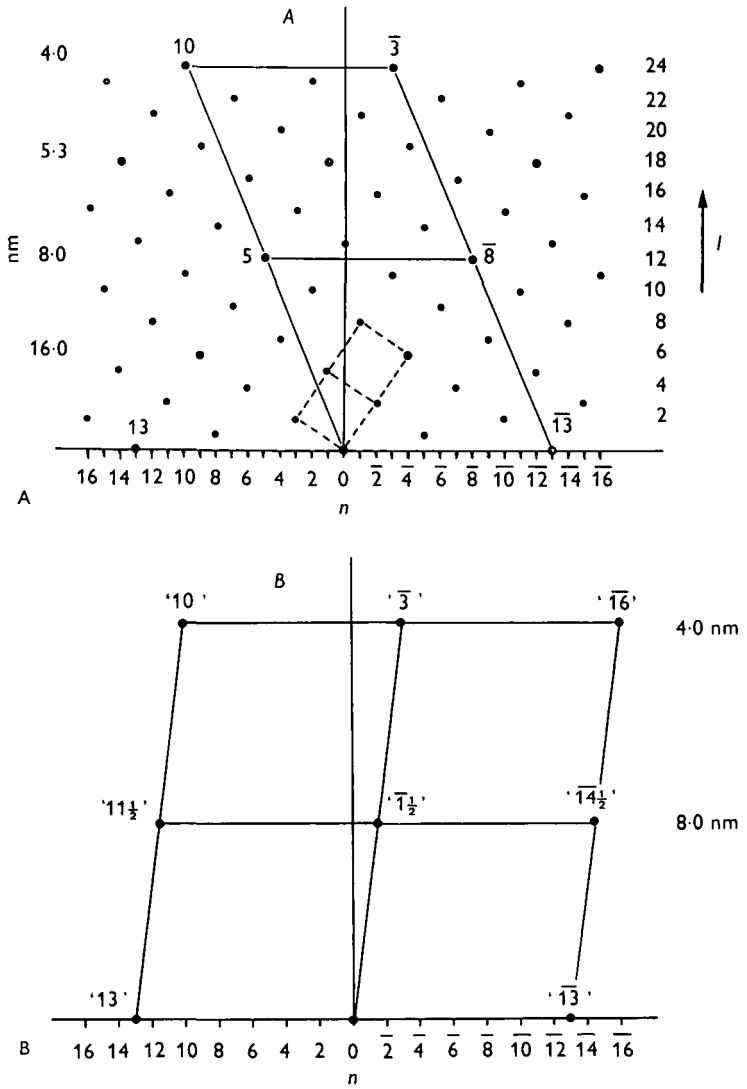

Fig. 5. A, the n-l plot for the A-tubule, n being the number of helices in a particular helical family and l the layer line number in the diffraction pattern. The numbering of l is based on a possible 96·0-nm longitudinal repeat. The solid lines indicate the unit cell of the reciprocal lattice when only the 4·0-nm and 8·0-nm periodicities are taken into account. If the surface lattice of the tubule were further organized into a superlattice of longitudinal repeat distance 96·0 nm owing to the helical attachment of additional components, the reciprocal unit cell would be defined by the dashed lines.

B, the equivalent of an n-l plot for the B-subfibre reciprocal lattice. For purposes of comparison with the A-subfibre, the reflexions are labelled with values of n as if the B-subfibre were also a complete 13-fold helical structure. The spacing of the reflexion labelled $n = -3$ on the 4·0-nm layer line is halved, rather than the one labelled $n = 10$. This leads to a different 8·0-nm unit cell from that of the A-subfibre.

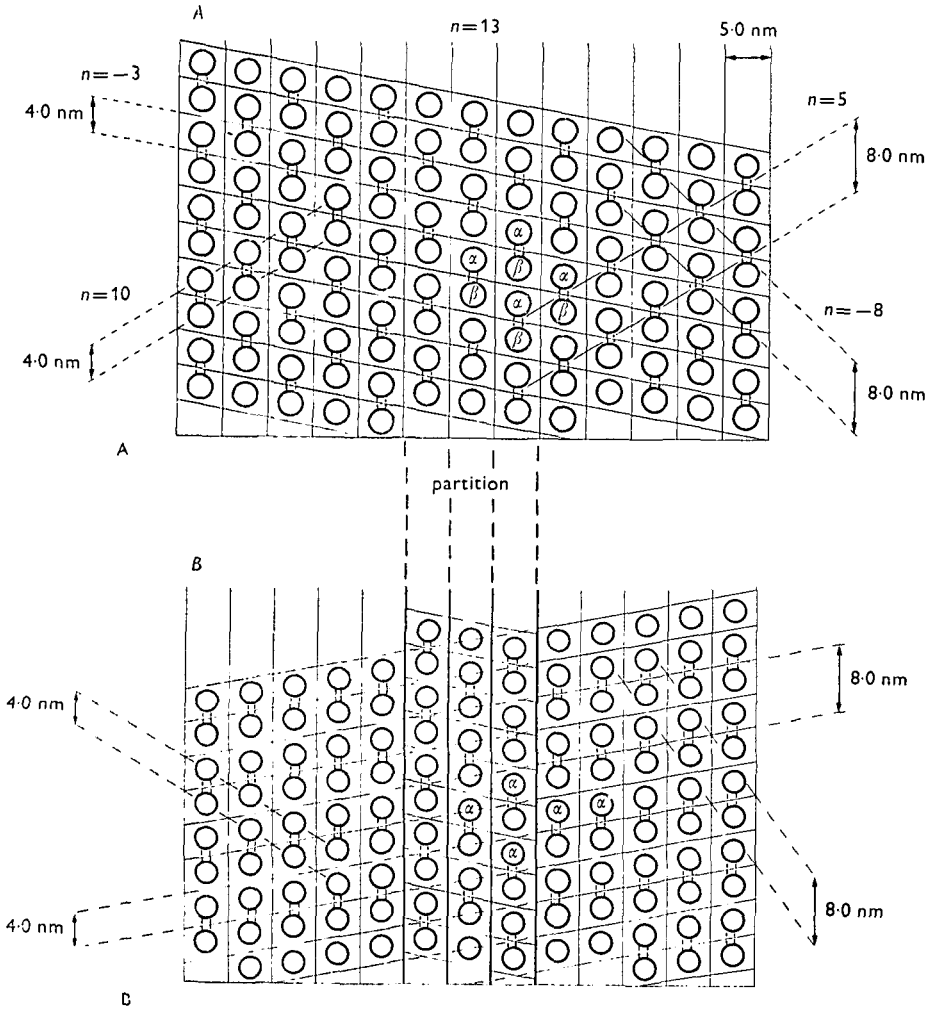

Fig. 6. A, the unrolled helical surface lattice which corresponds to the 8·0-nm period reciprocal lattice of Fig. 5A, drawn at a radius of about 8·0 nm, where the distance between adjacent protofilaments is 5·0 nm. The 5 most important families of helices in the lattice are indicated. They are labelled with the index n which gives the number of starts in the helical family. The sign of n gives the hand, positive being defined as right-handed. The lattice is basically the same as that shown by Grimstone & Klug (1966, fig. 1b), except that it has been drawn with the opposite hand and the 4·0-nm morphological units have been paired into dumb-bell-shaped dimers to produce the 8·0-nm periodicity. Here the lattice is meant to represent the A-tubule opened out as a sheet and viewed from the outside.

B, the surface lattice of the B-subfibre as seen from the inside. The central 3 filaments shown are part of the A-subfibre seen from the outside, as in A. The axial displacement between the dimers in the B-lattice and those in the A has been estimated from filtered images such as those shown in Fig. 11. Because the 4·0-nm lattices are of the same hand in both tubules (Linck & Amos, 1974), the helices slope in opposite directions in this view and the partition must represent a discontinuity in the B-lattice. The details of the arrangement of subunits at the seams and the way in which the two subfibres are joined have yet to be determined.

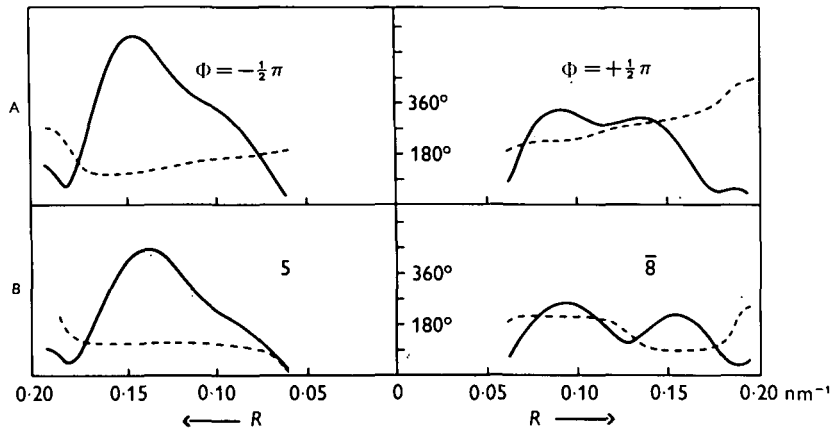

Fig. 7. A diagram to show the process of separating overlapping odd and even cylindrical harmonics on the same layer line of a helical diffraction pattern. The even function (made up of $J_8(2\pi Rr).e^{-i8\Phi}$ terms) is found by summing the complex values at corresponding points on the 2 sides of the layer line, the odd function (made up of $J_5(2\pi Rr).e^{i5\Phi}$ terms) by finding the differences between corresponding values (see footnote on p. 530). In A, the amplitudes of the original layer line (solid lines) are shown on an arbitrary scale; the phases (dashed lines) are plotted in degrees. In B, the separated functions are shown in positions relative to the meridian which correspond to the diffraction pattern of just the near side of the tubule.

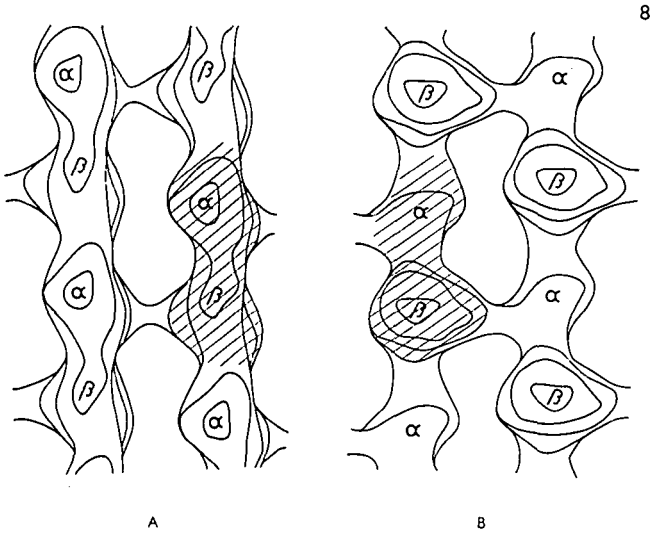

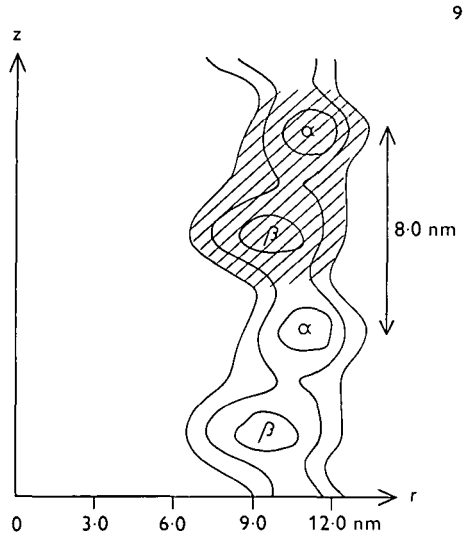

Fig. 8. Superimposed 'cylindrical sections' through 2 filaments of the 3-dimensional reconstructed image, a single contour having been drawn for each radius. A shows the map as viewed from the outside, with sections between radii of 9·6 and 12·0 nm; B shows the view from the inside, with sections between radii of 7·2 and 9·6 nm. A heterodimer is identified as a pair of peaks connected by the thicker bridge, and one is shown shaded.

Fig. 9. A radial section through the centre of a protofilament showing the radial zig-zag arrangement produced by the alternating morphological units.

Fig. 10. A, micrograph of intact doublet tubules from *Trichonympha* (Grimstone & Klug, 1966). The section of tubule shown outlined was densitometered so that the diffraction patterns shown in B to E could be calculated in a digital computer. × 180000.

B–E, computed diffraction patterns from the doublet in A. Only half of each pattern is shown. The computed intensities here (and those of the diffraction patterns and the filtered images of Fig. 11) were converted to a visual display using a cathode-ray-tube plotter (Gossling, 1967). B shows the diffraction pattern from the whole doublet. The main difference between this and the patterns from singlet A-tubules (see Figs. 2–4) is the presence of a pair of near-meridional peaks on the 8·0-nm layer line.

C is a repeat of B, on which are drawn both sides of the reciprocal lattice of the A-tubule, as in D, together with the 2 sides of a second lattice which includes the extra 8·0-nm peaks, as in E. The 2 lattices have the equatorial and 4·0-nm layer line peaks in common. The reason that the peaks do not all lie exactly on the points of a lattice is that the doublet fibre is reasonably well preserved and the subfibres are cylindrical rather than flat. There may also be different features at different radii.

D, diffraction pattern from just the A-subfibre of the doublet, including half of the partition. Apart from a small streak near the meridian on the 8·0-nm layer line, probably due to the discontinuity at the partition, the pattern on the 8·0 and 4·0-nm layer lines is virtually identical to those from singlet A-tubules.

E, diffraction pattern from the B-subfibre plus half of the partition. The near-meridional peaks are the strongest features of the 8·0-nm layer line, indicating that the B-subfibre has a different lattice from that of the A-subfibre.

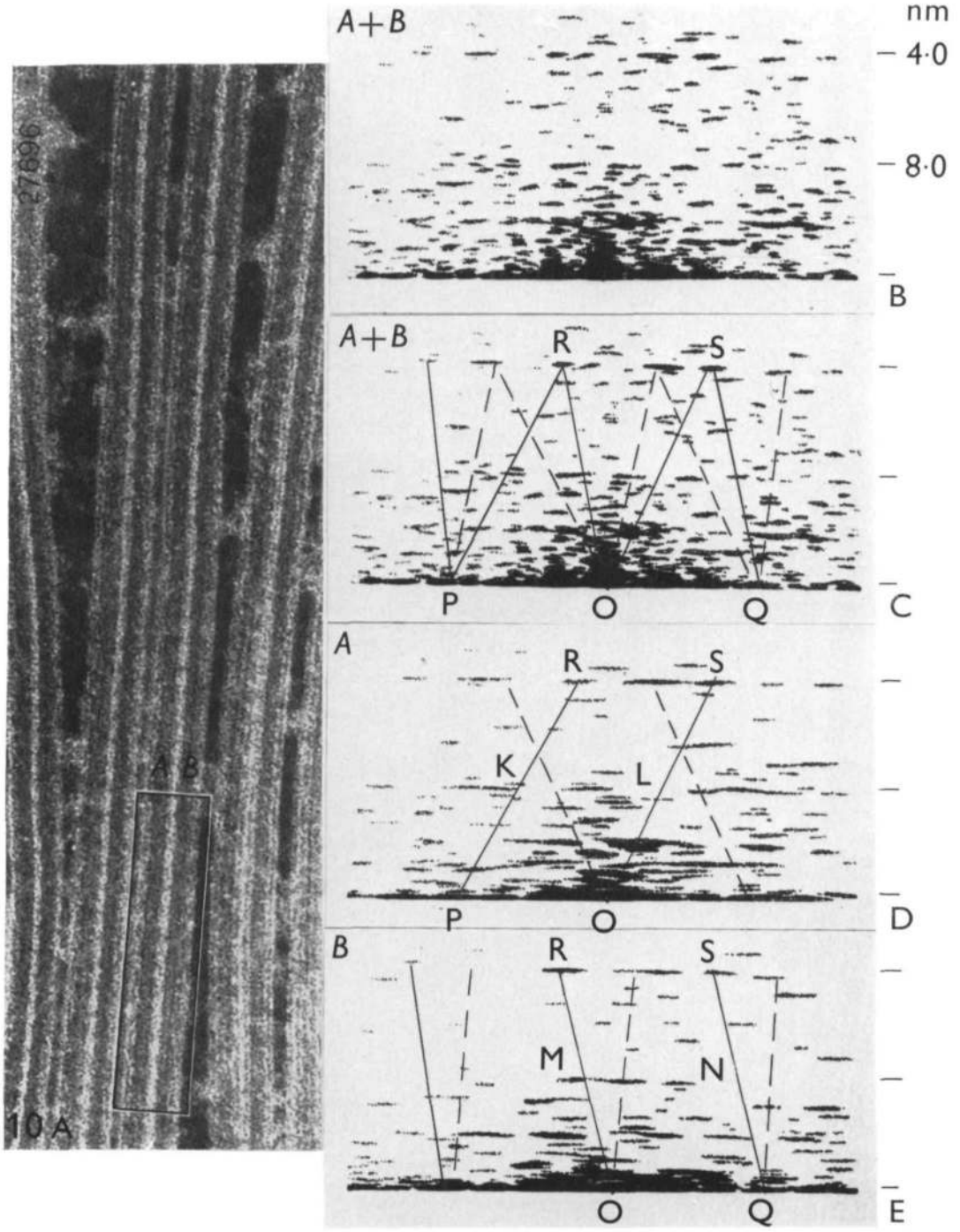
27696
A B
10 A
A+B
nm
4·0
8·0
B
A+B
R
S
P
O
Q
C
A
R
S
K
L
P
O
D
B
R
S
M
N
O
Q
E

Fig. 11. A, micrograph showing isolated doublets from *Trichonympha*, which have flattened on the grid and are therefore good subjects for 2-dimensional image filtering. × 180000.

B and D are the computed diffraction pattern (see legend to Fig. 10) obtained from the section of doublet outlined in A. B shows the mask used to produce the filtered image in C, while the mask in D was used to synthesize E. The equatorial peaks were included with half weight in both filtered images.

C and E are filtered images of part of the doublet tubule in A, showing the 2 separated sides of the image. The difference between the arrangements of dimers in the A- and B-subfibres can be seen quite clearly.

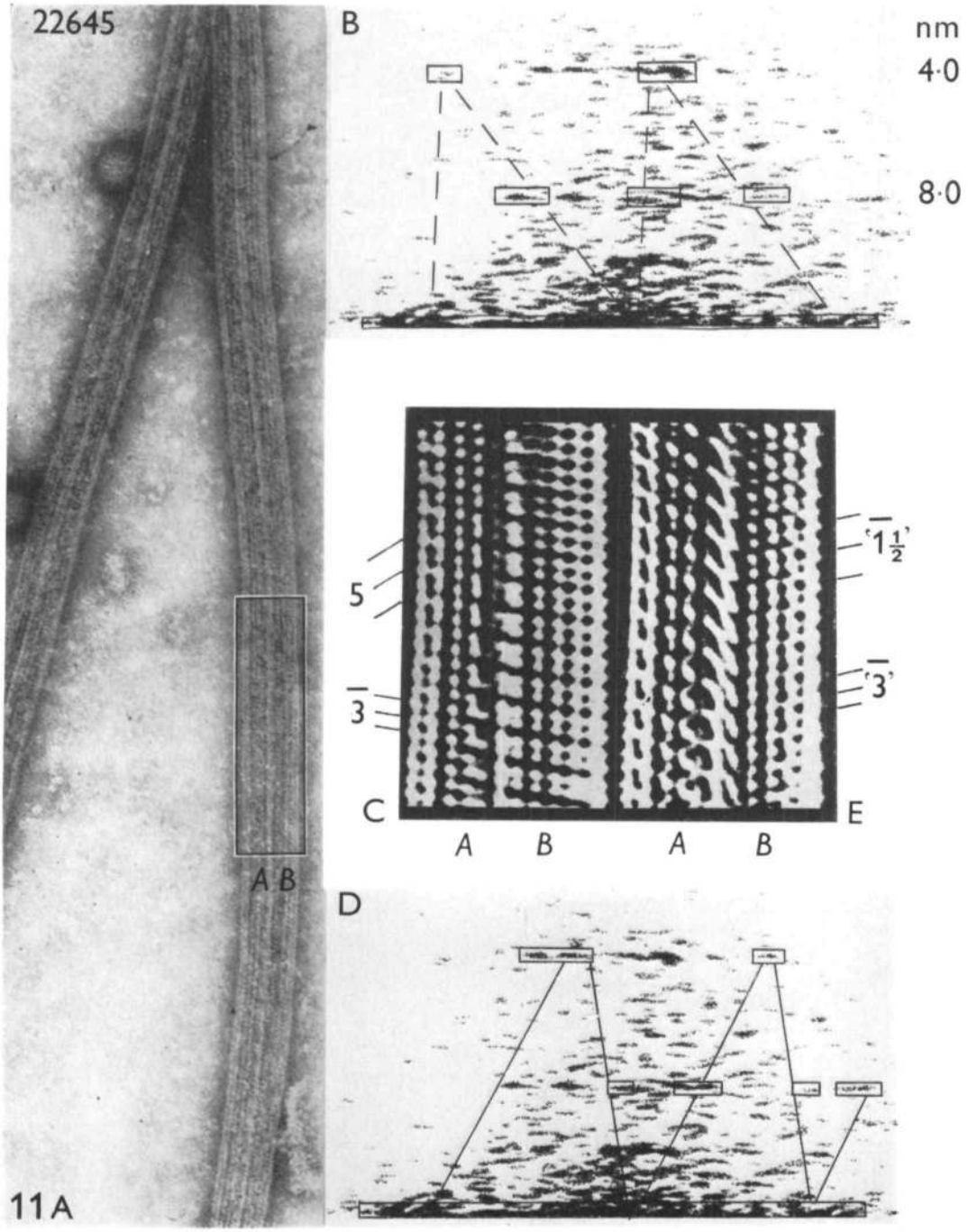
22645
A B
11A
B
nm
4·0
8·0
5
$\bar{3}$
C
A B A B
E
'$1\frac{1}{2}$'
'$\bar{3}$'
D

Fig. 12. A, micrograph (taken by H. P. Erickson) showing part of a B-subfibre (right) which has fallen away from the still intact A-tubule (left) to form a flat sheet of 10 protofilaments. × 300000.

B, diffraction pattern from part of the B-subfibre in A. The 2 peaks at a longitudinal spacing of 4·0 nm correspond exactly to those on the 4·0-nm layer lines of intact A- or B-subfibres (cf. Figs. 3, 4 and 10). At 8·0 nm, although the '$n = -1\frac{1}{2}$' and '$n = 11\frac{1}{2}$' peaks are very weak, there is a strong peak at '$n = -14\frac{1}{2}$' (cf. Fig. 5B).

C, optically filtered image of the B-tubule sheet obtained by masking out all but the strong peaks in B.

Fig. 13. A model of the 3-dimensional reconstruction of a singlet A-tubule which shows the 4·0- and 8·0-nm periodicities. The 2 types of 4·0-nm morphological unit are labelled α and β.

Fig. 14. Simple model showing the most probable arrangement of dimers in a doublet tubule (see also Figs. 6A, B), as deduced from filtered images (see Fig. 11C). The 4·0-nm lattices, which are marked by the oblique lines, have been drawn with identical parameters in the 2 subfibres and are approximately continuous across the seams. The 8·0-nm lattices, on the other hand, are quite different in the 2 subfibres.

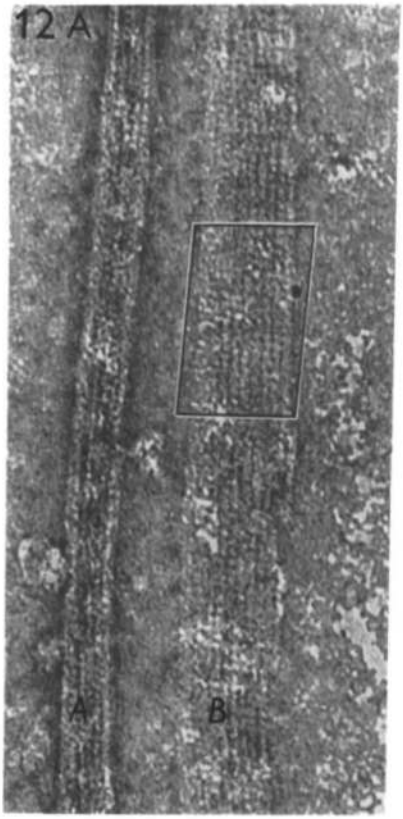
12 A
A
B

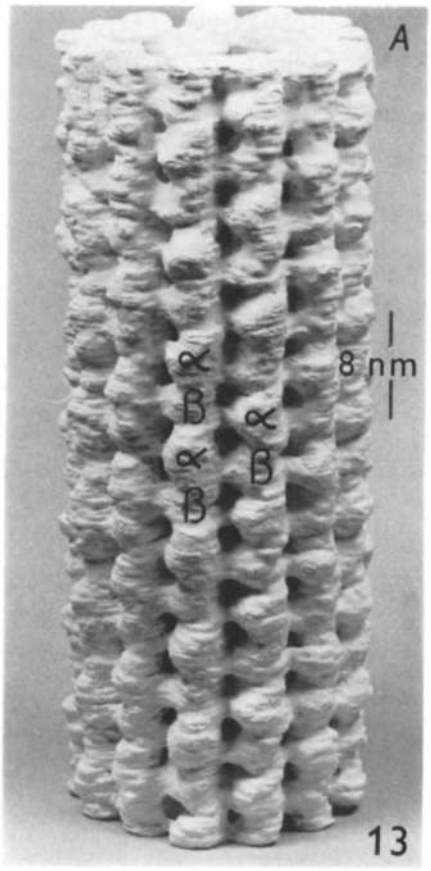
A
8 nm
α
β
α
β
α
β
13

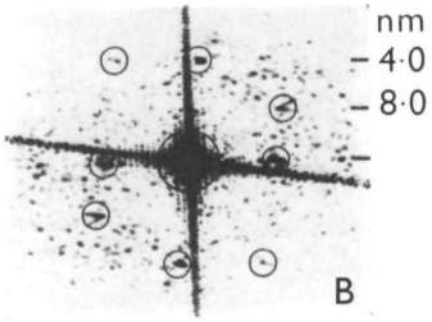
nm
– 4·0
– 8·0
B

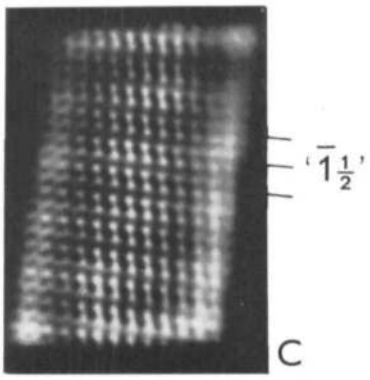
$(\bar{1}\frac{1}{2})$
C

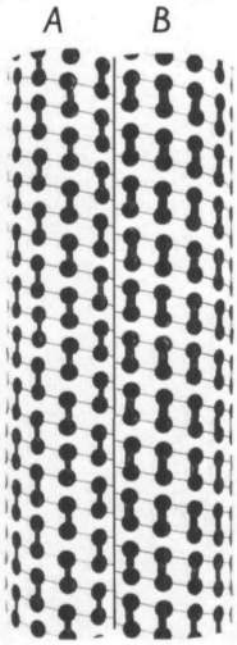
A
B
14